

Photoinduced Long-Range Magnetic Ordering of a Cobalt–Iron Cyanide

O. Sato,^{*,†} Y. Einaga,[‡] A. Fujishima,^{†,‡} and K. Hashimoto^{*,†,§}

Kanagawa Academy of Science and Technology, 1583 Iiyama Atsugi, Kanagawa 243-0279, Japan, Department of Applied Chemistry, The University of Tokyo, 7-3-1 Hongo, Bunkyo-ku, Tokyo 113-8656, Japan, and Research Center for Advanced Science and Technology, The University of Tokyo, 4-6-1 Komaba, Meguro-ku, Tokyo 153-8904, Japan

Received June 29, 1998

Two kinds of cobalt–iron cyanides ($\text{Rb}_{0.66}\text{Co}_{1.25}[\text{Fe}(\text{CN})_6]\cdot 4.3\text{H}_2\text{O}$ and $\text{Co}_{1.5}[\text{Fe}(\text{CN})_6]\cdot 6\text{H}_2\text{O}$) with different electronic structures have been investigated to understand the photoinduced long-range magnetic ordering. $\text{Rb}_{0.66}\text{Co}_{1.25}[\text{Fe}(\text{CN})_6]\cdot 4.3\text{H}_2\text{O}$ produces a photomagnetic effect, whereas $\text{Co}_{1.5}[\text{Fe}(\text{CN})_6]\cdot 6\text{H}_2\text{O}$ does not respond to light. FT-IR and Mössbauer studies revealed that their oxidation states are expressed as $\text{Rb}_{0.66}\text{Co}^{\text{II}}_{0.84}\text{Co}^{\text{III}}_{0.41}[\text{Fe}^{\text{II}}(\text{CN})_6]$ and $\text{Co}^{\text{II}}_{1.5}[\text{Fe}^{\text{III}}(\text{CN})_6]$, respectively. The difference in the oxidation states of the metal atoms in these two compounds has been explained by the Co coordination with H_2O or CN ligands. In the case of $\text{Rb}_{0.66}\text{Co}_{1.25}[\text{Fe}(\text{CN})_6]\cdot 4.3\text{H}_2\text{O}$, more CN ligands are involved in coordination than expected in the case of $\text{Co}_{1.5}[\text{Fe}(\text{CN})_6]\cdot 6\text{H}_2\text{O}$. A charge-transfer (CT) band from Fe^{II} to Co^{III} is observed at around 550 nm for $\text{Rb}_{0.66}\text{Co}_{1.25}[\text{Fe}(\text{CN})_6]\cdot 4.3\text{H}_2\text{O}$. The magnetism of $\text{Rb}_{0.66}\text{Co}_{1.25}[\text{Fe}(\text{CN})_6]\cdot 4.3\text{H}_2\text{O}$ changed from paramagnetic to ferrimagnetic due to the CT from Fe^{II} to Co^{III} when illuminated at low temperature. The Curie temperature after illumination was 22 K. This metastable state was stable for more than several days at 5 K. The metastable state was restored back to its original one when the sample was heated to 120 K. It is considered that the interconversion proceeded via a pronounced domain formation.

Introduction

The design of molecule-based compounds exhibiting spontaneous magnetization with high Curie temperature, T_c , is one of the main challenges in molecular materials science.^{1–4} The $\text{V}(\text{TCNE})_2\cdot\frac{1}{2}\text{CH}_2\text{Cl}_2$ compound has been reported to exhibit the highest T_c (above 350 K).³ All other high- T_c compounds are Prussian blue analogues such as $\text{V}[\text{Cr}(\text{CN})_6]_{0.86}\cdot 2.8\text{H}_2\text{O}$ ($T_c = 315$ K),⁵ $[\text{Cr}_{2.12}(\text{CN})_6]\cdot 2.8\text{H}_2\text{O}$ ($T_c = 270$ K),⁶ $[\text{Cr}_5(\text{CN})_{12}]\cdot 10\text{H}_2\text{O}$ ($T_c = 240$ K),⁷ and $(\text{Et}_4\text{N})_{1.25}\text{Mn}_{0.5}[\text{V}(\text{CN})_5]\cdot 2\text{H}_2\text{O}$ ($T_c = 230$ K).⁸

Recently, the development of new magnetic materials in which magnetic properties are combined with optical and

electrical properties has been extensively studied.^{6,9–13} We have been trying to make new types of magnets whose magnetic properties can be controlled by external stimuli. One of the most important challenges in the new field is the control of magnetic properties by light illumination. This subject is of considerable importance, because the photon mode allows us to access a variety of different types of materials with high speed and superior resolution. In our previous reports, we have shown that cobalt–iron cyanide exhibits photoinduced magnetization effects.⁹ In this work, we have attempted to explore the photomagnetic behavior of two types of materials, namely, $\text{Co}_{1.5}[\text{Fe}(\text{CN})_6]\cdot 6\text{H}_2\text{O}$ and $\text{Rb}_{0.66}\text{Co}_{1.25}[\text{Fe}(\text{CN})_6]\cdot 4.3\text{H}_2\text{O}$. The unit cell structure of these compounds is schematically shown in Figure 1. We have characterized these two cobalt–iron cyanides by various analytical techniques and also discussed the mechanism of the light-induced effects.

Experimental Section

Compound Preparation. $\text{Co}_{1.5}[\text{Fe}(\text{CN})_6]\cdot 6\text{H}_2\text{O}$. An aqueous solution of CoCl_2 (1 mM) was slowly added to a vigorously stirred aqueous

- [†] Kanagawa Academy of Science and Technology.
[‡] Department of Applied Chemistry, The University of Tokyo.
[§] Research Center for Advanced Science and Technology, The University of Tokyo.
- (1) Kahn, O. *Molecular Magnetism*; VCH: New York, 1993.
 - (2) (a) Kahn, O., Gatteschi, D., Miller, J. S., Palacio, F., Eds. *Magnetic Molecular Materials*; Kluwer: London, 1991; Vol. E198. (b) Iwamura, H.; Koga, N. *Acc. Chem. Res.* **1993**, *26*, 346. (c) Miller, J. S.; Epstein, A. J. *Angew. Chem., Int. Ed. Engl.* **1994**, *33*, 385. (d) Rajca, A. *Chem. Rev.* **1994**, *94*, 871. (e) Gatteschi, D. *Adv. Mater.* **1994**, *9*, 635. (f) Miller, J. S.; Epstein, A. J. *Chem. Eng. News* **1995**, *Oct. 2*, 30. (g) Turnbull, M. M., Sugimoto, T., Thompson, L. K., Eds. *Molecule-Based Magnetic Materials*; ACS Symposium Series 644; American Chemical Society: Washington, DC, 1996. (h) Iwamura, H.; Inoue, K.; Hayamizu, T. *Pure Appl. Chem.* **1996**, *68*, 243.
 - (3) Manriquez, J. M.; Yee, G. T.; Mclean, R. S.; Epstein, A. J.; Miller, J. S. *Science* **1991**, *252*, 1415.
 - (4) (a) Ito, A.; Suenaga, M.; Ono, K. *J. Chem. Phys.* **1968**, *48*, 3597. (b) Griebler, W. D.; Babel, D. Z. *Naturforsch* **1982**, *37B*, 832. (c) Babel, D. *Comments Inorg. Chem.* **1986**, *5*, 285. (d) Gadet, V.; Mallah, T.; Castro, I.; Veillet, P.; Verdager, M. *J. Am. Chem. Soc.* **1992**, *114*, 9214. (e) Entley, W. R.; Girolami, G. S. *Inorg. Chem.* **1994**, *33*, 5165. (f) Ohkoshi, S.; Sato, O.; Iyoda, T.; Fujishima, A.; Hashimoto, K. *Inorg. Chem.* **1997**, *36*, 268. (g) Ohkoshi, S.; Iyoda, T.; Fujishima, A.; Hashimoto, K. *Phys. Rev. B* **1997**, *56*, 11642.
 - (5) Ferlay, S.; Mallah, T.; Ouahes, R.; Veillet, P.; Verdager, M. *Nature* **1995**, *378*, 701.

- (6) Sato, O.; Iyoda, T.; Fujishima, A.; Hashimoto, K. *Science* **1996**, *271*, 49.
- (7) Mallah, T.; Thiebaut, S.; Verdager, M.; Veillet, P. *Science* **1993**, *262*, 1554.
- (8) Entley, W. R.; Girolami, G. S. *Science* **1995**, *268*, 397.
- (9) (a) Sato, O.; Iyoda, T.; Fujishima, A.; Hashimoto, K. *Science* **1996**, *272*, 704. (b) Sato, O.; Einaga, Y.; Iyoda, T.; Fujishima, A.; Hashimoto, K. *J. Electrochem. Soc.* **1997**, *144*, 11.
- (10) (a) Gu, Z. Z.; Sato, O.; Iyoda, T.; Hashimoto, K.; Fujishima, A. *Mol. Cryst. Liq. Cryst.* **1996**, *286*, 147. (b) Gu, Z. Z.; Sato, O.; Iyoda, T.; Hashimoto, K.; Fujishima, A. *J. Phys. Chem.* **1996**, *47*, 18289. (c) Gu, Z. Z.; Sato, O.; Iyoda, T.; Hashimoto, K.; Fujishima, A. *Chem. Mater.* **1997**, *9*, 1092.
- (11) Ohkoshi, S.; Yorozu, Y.; Sato, O.; Iyoda, T.; Fujishima, A.; Hashimoto, K. *Appl. Phys. Lett.* **1997**, *70*, 1040.
- (12) Nagai, K.; Iyoda, T.; Fujishima, A.; Hashimoto, K. *Solid State Commun.* **1997**, *102*, 809.
- (13) Sano, Y.; Tanaka, M.; Koga, N.; Matsuda, K.; Iwamura, H.; Rabu, P.; Drillon, M. *J. Am. Chem. Soc.* **1997**, *119*, 8246.

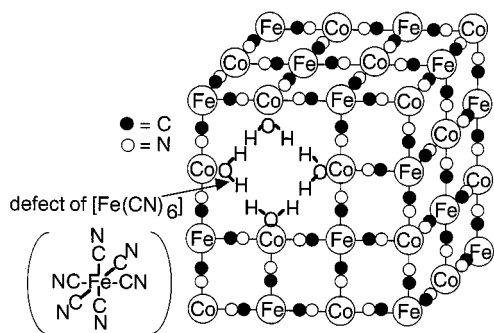


Figure 1. Unit cell of cobalt-iron cyanide. Certain $\text{Fe}(\text{CN})_6$ sites are vacant, and the bridging oxygen of H_2O fills the empty nitrogen end. Interstitial alkali metal cations have been omitted for clarity.

solution of $\text{K}_3\text{Fe}(\text{CN})_6$ (1 mM). The reaction produced a red precipitate. Anal. Calcd for $\text{Co}_{1.5}[\text{Fe}(\text{CN})_6] \cdot 6\text{H}_2\text{O}$: K, 0; Co, 21.64; Fe, 13.67; C, 17.64; N, 20.58; H, 2.97; Cl, 0. Found: K, 0.29; Co, 20.46; Fe, 12.91; C, 17.06; N, 19.78; H, 2.85; Cl, 0. (Co:Fe = 1.50:1).

$\text{Rb}_{0.66}\text{Co}_{1.25}[\text{Fe}(\text{CN})_6] \cdot 4.3\text{H}_2\text{O}$. An aqueous solution containing CoCl_2 (10 mM) and RbCl (1 M) was slowly added to a vigorously stirred aqueous solution containing $\text{K}_3\text{Fe}(\text{CN})_6$ (10 mM) and RbCl (1 M). The reaction produced a dark purple precipitate. Anal. Calcd for $\text{Rb}_{0.66}\text{Co}_{1.25}[\text{Fe}(\text{CN})_6] \cdot 4.3\text{H}_2\text{O}$: Rb, 13.4; Co, 17.6; Fe, 13.3; C, 17.18; N, 20.08; H, 2.07; Cl, 0. Found: Rb, 12.8; Co, 16.6; Fe, 12.7; C, 17.05; N, 19.62; H, 1.97; Cl, 0. (Rb:Co:Fe = 0.66:1.24:1).

Characterization. Physical Methods. The infrared (IR) spectra were measured with a model FT-IR 8900 μ (JASCO) and an FTS-40A (Bio-Rad) spectrophotometer at various temperatures. The powder samples were held by CaF_2 plates. IR measurement was not performed by the KBr method due to the interference of K^+ ions.¹⁴ The UV-vis spectra were monitored with a UV-3100 (Shimadzu) at various temperatures. At room temperature the spectra were measured by the diffuse reflectance method. At lower temperatures, the transmitted spectra were measured for the sample supported on commercial transparent tape. Temperature was controlled by a closed-cycle helium refrigerator (Iwatani Co., Ltd.) and a model 9650 temperature controller (Scientific Instruments). Powder X-ray diffraction patterns were measured with a RINT 2500V (Rigaku) at room temperature. Magnetic properties were investigated with a superconducting quantum interference device (SQUID) magnetometer (Quantum Design MPMS-5S). A Hg-Xe lamp (Yamashita Denso XFL-300L) was guided via optical fiber into the SQUID magnetometer for studying the photomagnetic effects. A powder sample (200–300 μg) was supported on a commercial transparent adhesive tape as thin as possible in order to efficiently illuminate the whole sample. The sample was placed on the edge of the optical fiber. An approximate value of the light intensity is mentioned in the text due to inhomogeneous illumination. The Mössbauer spectra (isomer shift vs metal Fe at room temperature) were measured using a Wissel MVT-1000 Mössbauer spectrometer with a $^{57}\text{Co}/\text{Rh}$ source in the transmission mode. The measurements at low temperature were performed with a closed-cycle helium refrigerator (Iwatani Co., Ltd.) or with liquid-helium cryostat.

Results and Discussion

The reaction of $\text{K}_3\text{Fe}(\text{CN})_6$ and CoCl_2 in aqueous solution typically produces red or purple precipitates. The stoichiometry and the electronic structure of the compounds strongly depend on the preparation conditions. In general, it is known that the single crystal of Prussian blue analogues is difficult to obtain due to the rapid reaction of the $\text{K}_3\text{Fe}(\text{CN})_6$ and CoCl_2 . Therefore, the powder form of the cobalt-iron cyanides has been characterized.

Table 1. Frequencies of CN Stretching, $\nu(\text{CN})$, of Prussian Blue Analogs and Their Related Compounds

compd	$\nu(\text{CN})$ (cm^{-1})	ref and notes
$\text{Fe}^{\text{II}}-\text{CN}-\text{Mn}^{\text{II}}$	2065	15
$\text{Fe}^{\text{II}}-\text{CN}-\text{Co}^{\text{II}}(\text{hs})$	2085	16
$\text{Fe}^{\text{II}}-\text{CN}-\text{Ni}^{\text{II}}$	2095	15
$\text{Fe}^{\text{II}}-\text{CN}-\text{Cu}^{\text{II}}$	2100	15
$\text{Fe}^{\text{II}}-\text{CN}-\text{Zn}^{\text{II}}$	2097	15
$\text{Fe}^{\text{III}}-\text{CN}-\text{Mn}^{\text{II}}$	2146	15
$\text{Fe}^{\text{III}}-\text{CN}-\text{Co}^{\text{II}}(\text{hs})$	2160	16
$\text{Fe}^{\text{III}}-\text{CN}-\text{Ni}^{\text{II}}$	2165	15
$\text{Fe}^{\text{III}}-\text{CN}-\text{Cu}^{\text{II}}$	2172	15
$\text{Fe}^{\text{III}}-\text{CN}-\text{Zn}^{\text{II}}$	2185	15
$\text{Co}_{1.5}[\text{Fe}(\text{CN})_6] \cdot 6\text{H}_2\text{O}$		
$\text{Fe}^{\text{III}}-\text{CN}-\text{Co}^{\text{II}}(\text{hs})$	2163	this work
$\text{Rb}_{0.66}\text{Co}_{1.25}[\text{Fe}(\text{CN})_6] \cdot 4.3\text{H}_2\text{O}$		
$\text{Fe}^{\text{III}}-\text{CN}-\text{Co}^{\text{III}}(\text{ls})$	2133	this work
after illumination		
$\text{Fe}^{\text{III}}-\text{CN}-\text{Co}^{\text{II}}(\text{hs})$	2169	this work
$\text{Fe}^{\text{II}}-\text{CN}-\text{Co}^{\text{II}}(\text{hs})$	2103	this work
$[(\text{NC})_5\text{Fe}^{\text{II}}-\text{CN}-\text{Co}^{\text{III}}(\text{ls})(\text{CN})_5]^{6-}$	2130	17

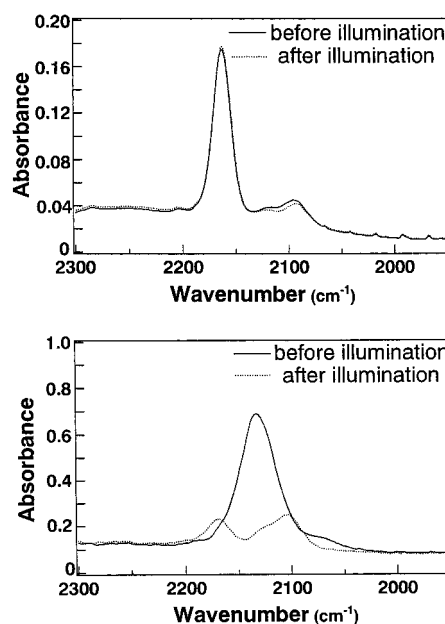


Figure 2. IR spectra of $\text{Co}_{1.5}[\text{Fe}(\text{CN})_6] \cdot 6\text{H}_2\text{O}$ (top) and $\text{Rb}_{0.66}\text{Co}_{1.25}[\text{Fe}(\text{CN})_6] \cdot 4.3\text{H}_2\text{O}$ (bottom) before and after light illumination at ca. 15 K.

IR and Mössbauer Spectra. The frequencies of CN stretching mode, $\nu(\text{CN})$, of $\text{Co}_{1.5}[\text{Fe}(\text{CN})_6] \cdot 6\text{H}_2\text{O}$ and $\text{Rb}_{0.66}\text{Co}_{1.25}[\text{Fe}(\text{CN})_6] \cdot 4.3\text{H}_2\text{O}$ are listed in Table 1, and their IR spectra in the region from 1950 to 2300 cm^{-1} are shown in Figure 2. The $\nu(\text{CN})$ values for Prussian blue analogues are also listed in Table 1.^{15,16} The $\nu(\text{CN})$ values of $\text{Fe}^{\text{II}}-\text{CN}-\text{M}^{\text{II}}$ and $\text{Fe}^{\text{III}}-\text{CN}-\text{M}^{\text{II}}$ appear in the region from 2065 to 2100 cm^{-1} and from 2146 to 2185 cm^{-1} , respectively. The $\nu(\text{CN})$ for $\text{Co}^{\text{II}}_2[\text{Fe}^{\text{II}}(\text{CN})_6]$ and $\text{K}_2\text{Co}^{\text{II}}[\text{Fe}^{\text{II}}(\text{CN})_6]$ with $\text{Fe}^{\text{II}}-\text{CN}-\text{Co}^{\text{II}}$ bond structure were observed at 2085 cm^{-1} .¹⁶ The $\nu(\text{CN})$ for a dinuclear compound, $[(\text{NC})_5\text{Fe}^{\text{II}}-\text{CN}-\text{Co}^{\text{III}}(\text{CN})_5]$, with $\text{Fe}^{\text{II}}-\text{CN}-\text{Co}^{\text{III}}$ bond structure was observed at 2130 cm^{-1} .^{17,18} These data indicate that the peaks at around 2163, 2133, and 2103 cm^{-1} observed with $\text{Co}_{1.5}[\text{Fe}(\text{CN})_6] \cdot 6\text{H}_2\text{O}$ and $\text{Rb}_{0.66}\text{Co}_{1.25}[\text{Fe}(\text{CN})_6] \cdot 4.3\text{H}_2\text{O}$ can be

(14) Reguela et al. claim that tribochemical reduction proceeds when the compound is mixed with KBr during the preparation of the IR pellet.¹⁵ We also observed a shift in the IR when it is mixed with KBr, KCl, etc. However, we believe the shift is induced by the penetration of ions (K^+ , etc.) into the interstitial sites, because we have observed cation exchange effects for electrochemically synthesized compounds.⁴²

(15) Bertrán, J. F.; Pascual, J. B.; Hernández, M.; Rodríguez, R. *React. Solids* **1988**, 5, 95.
 (16) Reguera, E.; Bertrán, J. F.; Díaz, C.; Blanco, J. *Hyperfine Interact.* **1990**, 53, 391.
 (17) Hester, R. E.; Nour, E. M. *J. Chem. Soc., Dalton Trans.* **1981**, 939.
 (18) Nakamoto, K. *Infrared and Raman Spectra of Inorganic and Coordination Compounds*; 4th ed.; Wiley: New York, 1986.

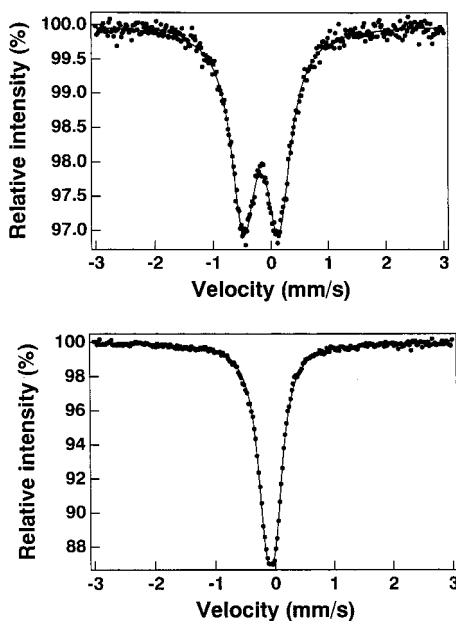


Figure 3. Mössbauer spectra for $\text{Co}_{1.5}[\text{Fe}(\text{CN})_6]\cdot 6\text{H}_2\text{O}$ (top) and $\text{Rb}_{0.66}\text{Co}_{1.25}[\text{Fe}(\text{CN})_6]\cdot 4.3\text{H}_2\text{O}$ (bottom) at room temperature.

assigned to the stretching of the CN bridge with the $\text{Fe}^{\text{III}}\text{—CN—Co}^{\text{II}}$, $\text{Fe}^{\text{II}}\text{—CN—Co}^{\text{III}}$, and $\text{Fe}^{\text{II}}\text{—CN—Co}^{\text{II}}$ bond structures, respectively.

The $\nu(\text{CN})$ value assigned to the $\text{Fe}^{\text{II}}\text{—CN—Co}^{\text{III}}$ moiety (2133 cm^{-1}) is higher by about 30 cm^{-1} compared with that assigned to the $\text{Fe}^{\text{II}}\text{—CN—Co}^{\text{II}}$ moiety (2103 cm^{-1}). The shift toward higher frequency is due to the change in the electronic states of Co cations from high-spin $\text{Co}^{\text{II}}(\text{hs}, t_{2g}^5e_g^2)$ to low-spin $\text{Co}^{\text{III}}(\text{ls}, t_{2g}^6e_g^0)$, where hs and ls represent high-spin and low-spin, respectively. Here, the decrease of the e_g electrons with antibonding character leads to the increase in back-bonding accompanied by a partial depopulation of the $\pi^*(\text{N—C})$ orbital in order to compensate the charge deficit at the central ion caused by the back-bonding. The decrease of the electrons in antibonding $\pi^*(\text{N—C})$ results in the shift of $\nu(\text{CN})$ toward higher frequency.

Mössbauer spectra support this assignment. The Mössbauer spectra of $\text{Co}_{1.5}[\text{Fe}(\text{CN})_6]\cdot 6\text{H}_2\text{O}$ and $\text{Rb}_{0.66}\text{Co}_{1.25}[\text{Fe}(\text{CN})_6]\cdot 4.3\text{H}_2\text{O}$ are shown in Figure 3. The Mössbauer parameters for these two compounds and their related ones are listed in Table 2.^{16,19–22} $\text{Co}_{1.5}[\text{Fe}(\text{CN})_6]\cdot 6\text{H}_2\text{O}$ has a doublet absorption peak with $\text{IS} = -0.17 \pm 0.01\text{ mm/s}$, $\text{QS} = 0.61 \pm 0.01\text{ mm/s}$, and $\Gamma = 0.51 \pm 0.01\text{ mm/s}$, which can be assigned to $\text{Fe}^{\text{III}}(\text{ls})$. $\text{Rb}_{0.66}\text{Co}_{1.25}[\text{Fe}(\text{CN})_6]\cdot 4.3\text{H}_2\text{O}$ also has a doublet absorption peak with $\text{IS} = -0.08 \pm 0.01\text{ mm/s}$, $\text{QS} = 0.16 \pm 0.01\text{ mm/s}$, and $\Gamma = 0.34 \pm 0.01\text{ mm/s}$, which can be assigned to $\text{Fe}^{\text{II}}(\text{ls})$.²³ Here, IS, QS, and Γ represent isomer shift, quadrupole splitting, and line width, respectively. The idealized electronic configurations of $\text{Fe}^{\text{III}}\text{—CN—Co}^{\text{II}}$ and $\text{Fe}^{\text{II}}\text{—CN—Co}^{\text{III}}$ in octahedral symmetry are expressed as $\text{Fe}^{\text{III}}(t_{2g}^5e_g^0)\text{—CN—Co}^{\text{II}}(\text{hs}, t_{2g}^5e_g^2)$ and $\text{Fe}^{\text{II}}(t_{2g}^6e_g^0)\text{—CN—Co}^{\text{III}}(\text{ls}, t_{2g}^6e_g^0)$, respectively. The IR and Mössbauer studies support the oxidation states of the metal atoms in $\text{Co}_{1.5}[\text{Fe}(\text{CN})_6]\cdot 6\text{H}_2\text{O}$ and $\text{Rb}_{0.66}\text{Co}_{1.25}[\text{Fe}(\text{CN})_6]\cdot 4.3\text{H}_2\text{O}$ as $\text{Co}^{\text{II}}_{1.5}[\text{Fe}^{\text{III}}(\text{CN})_6]$ and $\text{Rb}_{0.66}\text{Co}^{\text{III}}_{0.84}\text{Co}^{\text{II}}_{0.41}[\text{Fe}^{\text{II}}(\text{CN})_6]$, respec-

tively. The relatively broad CN stretching peaks of $\text{Rb}_{0.66}\text{Co}_{1.25}[\text{Fe}(\text{CN})_6]\cdot 4.3\text{H}_2\text{O}$ is due to the contribution from $\text{Fe}^{\text{II}}(t_{2g}^6e_g^0)\text{—CN—Co}^{\text{II}}(\text{hs}, t_{2g}^5e_g^2)$.

Powder X-ray Diffraction. Buser et al. have carried out a single-crystal analysis for Prussian blue, $\text{Fe}^{\text{III}}_4[\text{Fe}^{\text{II}}(\text{CN})_6]_3\cdot 15\text{H}_2\text{O}$,²⁴ which suggests that Prussian blue has a face-centered cubic (fcc) structure. The powder X-ray diffraction patterns of $\text{Co}_{1.5}[\text{Fe}(\text{CN})_6]\cdot 6\text{H}_2\text{O}$ and $\text{Rb}_{0.66}\text{Co}_{1.25}[\text{Fe}(\text{CN})_6]\cdot 4.3\text{H}_2\text{O}$ are consistent with the fcc structure. Their unit cell parameters are 10.32 and 9.96 Å, respectively. In general, $\text{Co}^{\text{III}}(\text{ls}, t_{2g}^6e_g^0)$ to $\text{Co}^{\text{II}}(\text{hs}, t_{2g}^5e_g^2)$ interconversion is characterized by elongation of the Co-to-ligand bond distance.²⁵ This is due to the fact that the e_g σ -antibonding orbitals in the $\text{Co}^{\text{III}}(\text{ls}, t_{2g}^6e_g^0)$ form are unoccupied but doubly occupied in the $\text{Co}^{\text{II}}(\text{hs}, t_{2g}^5e_g^2)$ form. Therefore, the change in the unit cell parameters of these compounds (10.32 to 9.96 Å) is mainly due to the variation in the Co–N bond length (Δr). It has been reported that the Fe^{II}–C and C–N bond lengths of $\text{Fe}^{\text{III}}_4[\text{Fe}^{\text{II}}(\text{CN})_6]_3\cdot 15\text{H}_2\text{O}$ are 1.92 and 1.13 Å, respectively.²⁴ Assuming that the bond lengths of Fe–C (Fe^{II}–C, Fe^{III}–C) and C–N of cobalt iron cyanide are equivalent with those of $\text{Fe}^{\text{III}}_4[\text{Fe}^{\text{II}}(\text{CN})_6]_3\cdot 15\text{H}_2\text{O}$, the Co^{II}(hs)–N bond length of $\text{Co}_{1.5}[\text{Fe}(\text{CN})_6]\cdot 6\text{H}_2\text{O}$ and Co^{III}(ls)–N bond length of $\text{Rb}_{0.66}\text{Co}_{1.25}[\text{Fe}(\text{CN})_6]\cdot 4.3\text{H}_2\text{O}$ are calculated to be 2.11 and 1.93 Å, respectively.²⁶ Their bond lengths are consistent with that of Co valence tautomeric compounds.²⁵ In general, the mean Δr variations for Co^{II} valence tautomeric compounds and Fe^{II}, Fe^{III}, and Co^{II} spin crossover complexes lie in the ranges of 0.16–0.22, 0.14–0.24, 0.10–0.18, and 0.09–0.13 Å, respectively.^{25,27} The Δr variation of the cobalt–iron cyanides (0.18 Å) is larger than the Δr of Co^{II} spin crossover complexes and falls within the Δr of Fe^{II} and Fe^{III} spin crossover and Co valence tautomeric compounds. This is because only one e_g orbital with antibonding character affects the Δr of Co^{II} spin crossover complexes, while two e_g orbitals affect the Δr of the others.

The elemental analysis shows that the number of $\text{Fe}(\text{CN})_6$ moieties is larger than that of Co cations in the two compounds. It has been reported that the Prussian blue analogues have $\text{Fe}(\text{CN})_6$ vacancies and the oxygen of H_2O fills the empty nitrogen sites of the vacancy (Figure 1).²⁴ For example, $\text{Fe}^{\text{III}}_4[\text{Fe}^{\text{II}}(\text{CN})_6]_3$ can be expressed by $\text{Fe}^{\text{III}}_4[\text{vacancy}][\text{Fe}^{\text{II}}(\text{CN})_6]_3$. The mean coordination of Fe^{III} is $\text{Fe}^{\text{III}}\text{N}_{4.5}\text{O}_{1.5}$, where N and O represent the nitrogen end of CN and the oxygen of H_2O . When this assumption is simply applied to the structural analysis, the two compounds prepared here can be expressed by $\text{Co}_{0.5}[\text{vacancy}]_{0.5}$ -

(23) We tried to fit the Mössbauer spectra of cobalt–iron cyanides, which have an $\text{Fe}^{\text{II}}(t_{2g}^6e_g^0)\text{—CN—Co}^{\text{III}}(\text{ls}, t_{2g}^6e_g^0)$ structure, with one line and by assuming a zero quadrupole interaction.²² However, it was found that the spectra could not be properly fit. Therefore, we have fit the Mössbauer spectra with a symmetric quadrupole doublet.

(24) Buser, H. J.; Schwarzenbach, D.; Petter, W.; Ludi, A. *Inorg. Chem.* **1977**, *16*, 2704.

(25) Adams, D. M.; Hendrickson, D. N. *J. Am. Chem. Soc.* **1996**, *118*, 11515.

(26) To clarify the structure of $\text{Co}_{1.5}[\text{Fe}(\text{CN})_6]\cdot 6\text{H}_2\text{O}$ and $\text{Rb}_{0.66}\text{Co}_{1.25}[\text{Fe}(\text{CN})_6]\cdot 4.3\text{H}_2\text{O}$, we have recently measured EXAFS spectra. Since they are described elsewhere (Yokoyama, T.; Ohta, T.; Sato, O.; Hashimoto K. *Phys. Rev. B.* **1998**, *58*, 8257), the bond lengths in $\text{Co}_{1.5}[\text{Fe}(\text{CN})_6]\cdot 6\text{H}_2\text{O}$ and $\text{Rb}_{0.66}\text{Co}_{1.25}[\text{Fe}(\text{CN})_6]\cdot 4.3\text{H}_2\text{O}$ are given here. $\text{Co}_{1.5}[\text{Fe}(\text{CN})_6]\cdot 6\text{H}_2\text{O}$: Fe–C = 1.915 Å, Fe–N = 3.043 Å, Fe–Co = 4.98 Å (from Fe K-edge EXAFS); Co–N = 1.933 Å, Co–C = 3.084 Å, Co–Fe = 5.00 Å (from Co K-edge EXAFS). $\text{Rb}_{0.66}\text{Co}_{1.25}[\text{Fe}(\text{CN})_6]\cdot 4.3\text{H}_2\text{O}$: Fe–C = 1.933 Å, Fe–N = 3.052 Å, Fe–Co = 5.17 Å (from Fe K-edge EXAFS); Co–N = 2.110 Å, Co–C = 3.243 Å, Co–Fe = 5.20 Å (from Co K-edge EXAFS). These data clearly show that the differences of the unit cell parameters between $\text{Co}_{1.5}[\text{Fe}(\text{CN})_6]\cdot 6\text{H}_2\text{O}$ and $\text{Rb}_{0.66}\text{Co}_{1.25}[\text{Fe}(\text{CN})_6]\cdot 4.3\text{H}_2\text{O}$ mainly arise from the change in the Co–N bond length.

(27) Zarembowitch, J. *New J. Chem.* **1992**, *16*, 255.

(19) Monaghan, C. P.; Fanning, J. C. *J. Phys. Chem.* **1978**, *82*, 2, 1045.

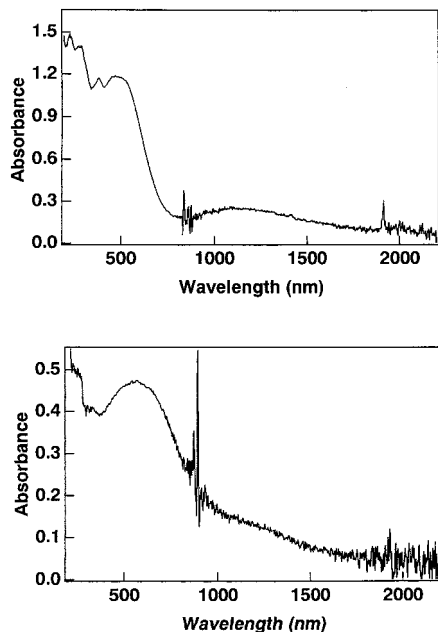
(20) Reguera, E.; Bertrán, J. F. *Hyperfine Interact.* **1994**, *88*, 49.

(21) Maer, K., Jr.; Beasley, M. L.; Collins, R. L.; Milligan, W. O. *J. Am. Chem. Soc.* **1968**, *90*, 3201.

(22) Einaga, Y.; Sato, O.; Iyoda, T.; Kobayashi, Y.; Ambe, F.; Hashimoto, K.; Fujishima, A. *Chem. Lett.* **1997**, 289.

Table 2. Mössbauer Parameters (Isomer Shift vs Metal Fe at Room Temperature)

compd	IS (mm/s)	QS (mm/s)	Γ (mm/s)	ref
$K_4Fe(CN)_6$	-0.031			19
$K_3Fe(CN)_6$	-0.122	0.285	0.242	20
$Co^{II}_2[Fe^{II}(CN)_6]$	-0.01			21
$Co^{II}_2[Fe^{II}(CN)_6]$	-0.085		0.320	16
$Co^{II}_3[Fe^{III}(CN)_6]_2$	-0.08	0.85		21
$Co^{II}_3[Fe^{III}(CN)_6]_2$	-0.151	0.408	0.353	16
$Co_{1.5}[Fe(CN)_6] \cdot 6H_2O = Co^{II}_3[Fe^{III}(CN)_6]_2$ (293 K)	-0.17 ± 0.01	0.61 ± 0.01	0.51 ± 0.01	this work
$Rb_{0.66}Co_{1.25}[Fe(CN)_6] \cdot 4.3H_2O$ (293 K)	-0.08 ± 0.01	0.16 ± 0.01	0.34 ± 0.01	this work
before illumination (25 K)	0.02 ± 0.01	0.15 ± 0.01	0.44 ± 0.01	this work
after illumination (25 K)	0.09 ± 0.01	1.13 ± 0.01	0.67 ± 0.01	this work

**Figure 4.** UV-vis spectra for $Co_{1.5}[Fe(CN)_6] \cdot 6H_2O$ (top) and $Rb_{0.66}Co_{1.25}[Fe(CN)_6] \cdot 4.3H_2O$ (bottom) at room temperature. The sharp oscillation around 830 nm is due to the change in the light source of the UV-vis spectrometer.

$Co[Fe(CN)_6] \cdot 6H_2O$ and $Rb_{0.66}Co_{0.25}[vacancy]_{0.25}Co[Fe(CN)_6] \cdot 4.3H_2O$. The mean coordination of Co in each compound is CoN_4O_2 and $CoN_{4.8}O_{1.2}$, respectively. The coordination of Fe is always maintained as FeC_6 in the Prussian blue analogues, where C represents the carbon end of CN.

The ligand field for nitrogen of CN is slightly higher than H_2O in the spectrochemical series. The difference in the ligand field of Co should affect the electronic structure of these compounds. The strong ligand field favors a low-spin state of Co ion rather than a high-spin state. Therefore, the electronic state of $Fe^{II}(t_{2g}^6e_g^0) - CN - Co^{III}(1s, t_{2g}^6e_g^0)$ is more stabilized as the number of vacancies decreases. As a consequence, $Co_{1.5}[Fe(CN)_6] \cdot 6H_2O$ with a relatively weak ligand field of Co cations procures the $Fe^{III}(t_{2g}^5e_g^0) - CN - Co^{II}(hs, t_{2g}^5e_g^2)$ state and $Rb_{0.66}Co_{1.25}[Fe(CN)_6] \cdot 4.3H_2O$ with a relatively strong ligand field takes the $Fe^{II}(t_{2g}^6e_g^0) - CN - Co^{III}(1s, t_{2g}^6e_g^0)$ state.²⁸

UV-Vis Electronic Absorption Spectra.²⁹ The optical absorption spectra of the present two compounds are shown in Figure 4. The red compound, $Co_{1.5}[Fe(CN)_6] \cdot 6H_2O$, has broad absorption peaks at around 1200, 470, and 380 nm. The spectrum seems to be the superposition of the spectrum of $K_3Fe^{III}(CN)_6$ and $Co^{II}(hs)$. The absorption at 1200 and 470 nm can be attributed to the d-d transitions of $Co^{II}(hs)$, and the

absorption at 380 nm is due to the charge-transfer band of $Fe(CN)_6^{3-}$. The purple compound, $Rb_{0.66}Co_{1.25}[Fe(CN)_6] \cdot 4.3H_2O$, has only one broad absorption peak at around 550 nm. The spectrum does not seem to be the simple superposition of the spectrum of $K_4Fe(CN)_6$ and $Co^{III}(1s)$, which indicates that $Rb_{0.66}Co_{1.25}[Fe(CN)_6] \cdot 4.3H_2O$ is a class II compound under the classification of Robin and Day.³⁰ This means that an electron is mainly trapped on Fe but is partially located on Co. We assign the broad band at 550 nm to the charge-transfer (CT) band from Fe^{II} to $Co^{III}(1s)$. The band structure calculation reported by Yoshizawa et al. also suggests that the absorption corresponds to the CT from Fe^{II} to Co^{III} .³¹ It is also important to note that several dinuclear compounds with $Fe^{II}-CN-Co^{III}(1s)$ structure have the CT bands in the 385–565 nm range.^{32–36}

Magnetic Properties. There are several reports available on the magnetic properties of $Co^{II}_{1.5}[Fe^{III}(CN)_6]$.^{37–39} The magnetic properties of our samples are shown in Figures 5–7. The product of the molar magnetic susceptibility and temperature, $\chi_M T$, versus temperature plot of $Co^{II}_{1.5}[Fe^{III}(CN)_6] \cdot 6H_2O$ first decreased upon cooling and then increased at lower temperatures (Figure 5), indicating a short-range antiferromagnetic interaction between paramagnetic centers bearing different numbers of unpaired electrons (ferrimagnetism). The Curie constant (C) and the Weiss constant (Θ) are $5.4 \text{ cm}^3 \text{ mol}^{-1} \text{ K}$ and -15 K , respectively. The field-cooled magnetization (FCM) versus temperature plots at H (magnetic field) = 0.5 mT displayed an abrupt break at $T_c = 16 \text{ K}$ (Figure 6). The field dependence of the magnetization (5 K) yielded a magnetization at $H = 5 \text{ T}$ of about $2.8 \mu_B/Co^{II}_{1.5}[Fe^{III}(CN)_6] \cdot 6H_2O$ (Figure 7). The magnetic hysteresis loop at 5 K yielded a remnant magnetization (M_r) of $3600 \text{ cm}^3 \text{ mol}^{-1} \text{ G}$ and a coercive field (H_c) of 480 G.

By neglect of the interaction between the next-nearest neighbors, the exchange interactions in the present compounds can be divided into two types. The interaction between the t_{2g} orbital of Fe^{III} and the e_g orbital of $Co^{II}(hs)$, which are orthogonal

- (30) Robin, M. B.; Day, P. *Adv. Inorg. Chem. Radiochem.* **1967**, *10*, 247.
 (31) Yoshizawa, K.; Mohri, F.; Nuspl, G.; Yamabe, T. *J. Phys. Chem. B.* **1998**, *102*, 5432.
 (32) Vogler, A.; Kunkely, H. *Ber. Bunsen-Ges. Phys. Chem.* **1975**, *79*, 301.
 (33) Hester, R. E.; Nour, E. M. *J. Chem. Soc., Dalton Trans.* **1981**, 939.
 (34) Bagger, S.; Stoltze, P. *Acta Chem. Scand. A* **1983**, *37*, 247.
 (35) Bagger, S.; Gibson, K. *Acta Chem. Scand.* **1973**, *27*, 3227.
 (36) Visalakshi, G.; Venkateswarlu K. S. *Proc. Indian Acad. Sci.* **1982**, *91*, 213.
 (37) (a) Hoden, A. N.; Matthias, B. T.; Anderson, P. W.; Lewis, H. W. *Phys. Rev.* **1956**, *102*, 1463. (b) Bozorth, R. M.; Williams, H. J.; Walsh, D. E. *Phys. Rev.* **1956**, *103*, 572.
 (38) (a) Gadet, V.; Bujoli, D. M.; Force, L.; Verdaguier, M.; Malkhi, K. E.; Deroy, A.; Besse, J. P.; Chappert, C.; Veillet, P.; Renard, J. P.; Beauvillain, P. In *Magnetic Molecular Materials*; Kahn, O.; Gatteschi, D.; Miller, J. S.; Palacio, F., Eds.; Kluwer: London, 1991; Vol. E198, p 281. (b) Verdaguier, M.; Mallah, T.; Gadet, V.; Castro, I.; Helary, C.; Thiebaut, S.; Veillet, P. In *Contributions to Development of Coordination Chemistry*; Ondrejovic, G.; Sirota, A., Eds.; Slovak Technical University Press: Bratislava, 1993; p 19.
 (39) Juszczak, S.; Johansson, C.; Hanson, M.; Ratuszna, A.; Malecki, G. *J. Phys. Condens. Matter* **1994**, *6*, 5697.

(28) Verdaguier, M. *Science*, **1996**, *272*, 698.(29) Figgis, B. N. *Introduction to Ligand Fields*; John Wiley & Sons: New York, 1970.

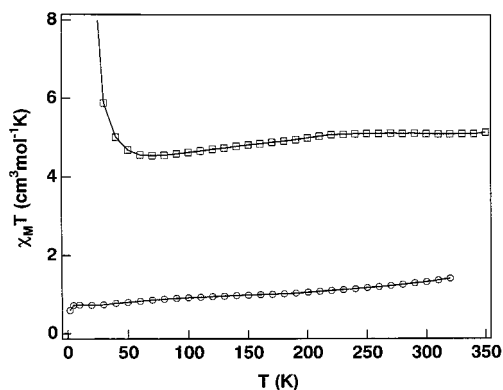


Figure 5. $\chi_M T$ vs temperature plots for $\text{Co}_{1.5}[\text{Fe}(\text{CN})_6] \cdot 6\text{H}_2\text{O}$ (\square) and $\text{Rb}_{0.66}\text{Co}_{1.25}[\text{Fe}(\text{CN})_6] \cdot 4.3\text{H}_2\text{O}$ (\circ).

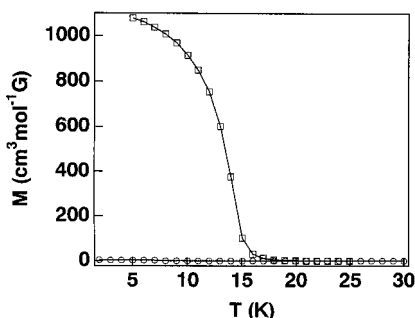


Figure 6. Field-cooled magnetization (FCM) vs T at $H = 0.5$ mT for $\text{Co}_{1.5}[\text{Fe}(\text{CN})_6] \cdot 6\text{H}_2\text{O}$ (\square) and $\text{Rb}_{0.66}\text{Co}_{1.25}[\text{Fe}(\text{CN})_6] \cdot 4.3\text{H}_2\text{O}$ (\circ) at 5 K.

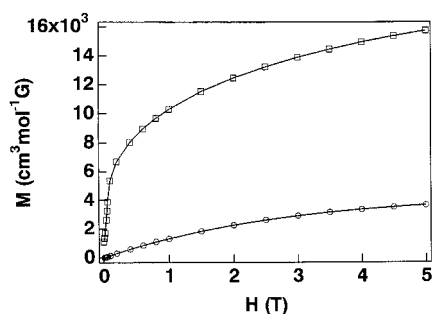


Figure 7. Field dependence of the magnetization for $\text{Co}_{1.5}[\text{Fe}(\text{CN})_6] \cdot 6\text{H}_2\text{O}$ (\square) and $\text{Rb}_{0.66}\text{Co}_{1.25}[\text{Fe}(\text{CN})_6] \cdot 4.3\text{H}_2\text{O}$ (\circ) at 5 K.

to each other, is ferromagnetic. The other interaction between the t_{2g} orbital of Fe^{III} and t_{2g} orbital of $\text{Co}^{\text{II}}(\text{hs})$, which are overlapped with each other, gives rise to antiferromagnetic character. When the ferromagnetic and antiferromagnetic interactions are superimposed, the antiferromagnetic term, in general, dominates the interactions.^{1,7} Therefore, ferrimagnetic properties are expected for the cobalt–iron cyanide, which is consistent with the observed magnetic properties of $\text{Co}_{1.5}[\text{Fe}(\text{CN})_6] \cdot 6\text{H}_2\text{O}$.

The $\chi_M T$ values of $\text{Rb}_{0.66}\text{Co}_{1.25}[\text{Fe}(\text{CN})_6] \cdot 4.3\text{H}_2\text{O}$ are quite small compared with those of $\text{Co}_{1.5}[\text{Fe}(\text{CN})_6] \cdot 6\text{H}_2\text{O}$ over all the temperature range (Figure 5), because they are mainly constituted from the diamagnetic component $\text{Fe}^{\text{II}}(t_{2g}^6 e_g^0) - \text{CN} - \text{Co}^{\text{III}}(1s, t_{2g}^6 e_g^0)$. The small amounts of Co^{II} ions in $\text{Rb}_{0.66}\text{Co}_{1.25}[\text{Fe}^{\text{II}}(\text{CN})_6]$ are responsible for the paramagnetic character. An FCM versus temperature plot for $\text{Rb}_{0.66}\text{Co}_{1.25}[\text{Fe}(\text{CN})_6] \cdot 4.3\text{H}_2\text{O}$ displayed no break between 2 K and room temperature (Figure 6). The field dependence of the magnetization yielded a magnetization at $H = 5$ T of about $0.66 \mu_B$ at 5 K per $\text{Rb}_{0.66}\text{Co}_{1.25}[\text{Fe}^{\text{II}}(\text{CN})_6]$ (Figure 7). The magnetic hysteresis

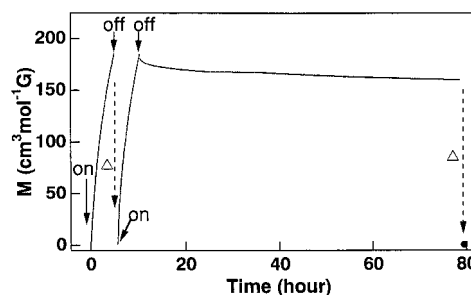


Figure 8. Change in the magnetization for $\text{Rb}_{0.66}\text{Co}_{1.25}[\text{Fe}(\text{CN})_6] \cdot 4.3\text{H}_2\text{O}$ at $H = 0.5$ mT and $T = 5$ K during light illumination and after thermal treatment; on, off, and Δ represent light on, light off, and thermal treatment at 150 K.

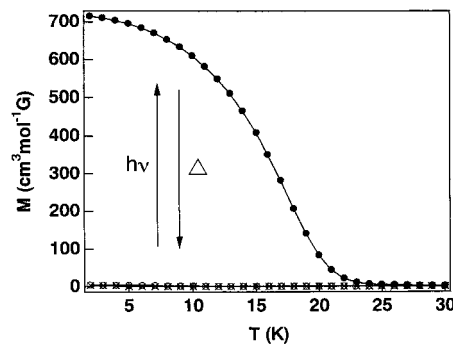


Figure 9. Field-cooled magnetization (FCM) curves for $\text{Rb}_{0.66}\text{Co}_{1.25}[\text{Fe}(\text{CN})_6] \cdot 4.3\text{H}_2\text{O}$ before and after light illumination ($h\nu$) at $H = 0.5$ mT: \circ , before light illumination; \bullet , after light illumination; \times , after thermal treatment at 150 K; (\circ and \times fall on the same line.) Δ represents thermal treatment.

loop could not be observed even at 5 K, which is characteristic of a paramagnetic material.

Effect of Illumination. The ferrimagnet, $\text{Co}_{1.5}[\text{Fe}(\text{CN})_6] \cdot 6\text{H}_2\text{O}$, did not show any photoeffect during magnetic measurements. Conversely, the paramagnetic compound, $\text{Rb}_{0.66}\text{Co}_{1.25}[\text{Fe}(\text{CN})_6] \cdot 4.3\text{H}_2\text{O}$, showed a strong response upon irradiation. The magnetization value of $\text{Rb}_{0.66}\text{Co}_{1.25}[\text{Fe}(\text{CN})_6] \cdot 4.3\text{H}_2\text{O}$ at $H = 0.5$ mT increased significantly under illumination at 5 K. The time dependence of the change in the magnetization value under light illumination (500–750 nm, light intensity = ca. 0.1 mW/cm^2 , sample mass = $268 \mu\text{g}$) is shown in Figure 8. The magnetization value started to increase upon illumination, indicating that a long-range magnetic ordering is induced by the light illumination. The light was turned off, and the magnetization was observed to be stable for several days. The original magnetization value at 5 K before illumination was recovered, when the sample was heated to 150 K (thermal treatment). This phenomenon can be repeated for several times. The light-induced persistent change in magnetization could be induced by any wavelength in the visible region, indicating that this effect is triggered by the excitation of the CT band. The light intensity in Figure 8 was reduced to 0.1 mW/cm^2 in order to clearly show the change in the magnetization during light illumination. Therefore, no saturation in the magnetization was attained even after illumination for 5 h. Basically, the increase in the magnetization is faster with an increase in the light intensity. The interconversion was completed below 10 min when white light at 20 mW/cm^2 was used. Figure 8 also shows the time dependence of the decrease in the magnetization at 5 K after the light is turned off. The FCM was measured as a function of temperature before and after the light illumination at 5 K (Figure 9). The Curie temperature was 22 K after illumination for about 40 min (500–750 nm, light intensity =

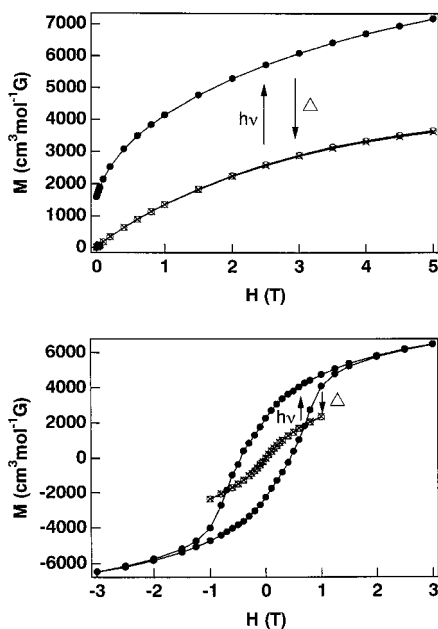
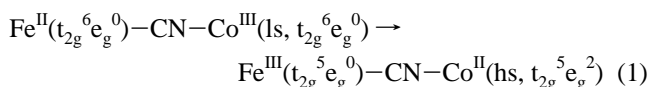


Figure 10. Top: Field dependence of the magnetizations for $\text{Rb}_{0.66}\text{Co}_{1.25}[\text{Fe}(\text{CN})_6]\cdot 4.3\text{H}_2\text{O}$ before and after light illumination ($h\nu$) at 2 K. Bottom: Hysteresis loops for $\text{Rb}_{0.66}\text{Co}_{1.25}[\text{Fe}(\text{CN})_6]\cdot 4.3\text{H}_2\text{O}$ at 2 K. \circ , before light illumination; \bullet , after light illumination; \times after thermal treatment at 150 K. (\circ and \times fall on the same line.) Δ represents thermal treatment.

ca. $7 \text{ mW}/\text{cm}^2$, sample mass = $251.5 \mu\text{g}$). The field dependence of the magnetization at 2 K is shown in Figure 10. The magnetization at $H = 5 \text{ T}$ yielded about $1.32 \mu_B/\text{Rb}_{0.66}\text{Co}_{1.25}[\text{Fe}(\text{CN})_6]$ after the illumination. Magnetic hysteresis after the illumination at 2 K yielded M_r of $2260 \text{ cm}^3 \text{ mol}^{-1} \text{ G}$ and H_c of 4500 G. Similar light-induced phenomena (enhanced magnetization) were observed even at 100 K.

The IR spectra at 12 K before and after light illumination are shown in Figure 2. Upon irradiation at 5 K for 10 min (white light, light intensity = ca. $20 \text{ mW}/\text{cm}^2$), the intensity of the peak at 2133 cm^{-1} disappeared almost completely and the peaks at 2169 and 2103 cm^{-1} appeared for $\text{Rb}_{0.66}\text{Co}_{1.25}[\text{Fe}(\text{CN})_6]\cdot 4.3\text{H}_2\text{O}$. The $\nu(\text{CN})$ peaks at 2169 , 2133 , and 2103 cm^{-1} , are assigned to $\text{Fe}^{\text{III}}(\text{t}_{2g}^5 \text{e}_g^0)\text{—CN—Co}^{\text{II}}(\text{hs}, \text{t}_{2g}^5 \text{e}_g^2)$, $\text{Fe}^{\text{II}}(\text{t}_{2g}^6 \text{e}_g^0)\text{—CN—Co}^{\text{III}}(\text{ls}, \text{t}_{2g}^6 \text{e}_g^0)$, and $\text{Fe}^{\text{II}}(\text{t}_{2g}^6 \text{e}_g^0)\text{—CN—Co}^{\text{II}}(\text{hs}, \text{t}_{2g}^5 \text{e}_g^2)$, respectively. This means that the light illumination induced the CT from Fe^{II} to $\text{Co}^{\text{III}}(\text{ls})$ for $\text{Rb}_{0.66}\text{Co}_{1.25}[\text{Fe}(\text{CN})_6]\cdot 4.3\text{H}_2\text{O}$. The process could be expressed by



Mössbauer spectra support these assignments (Figure 11). Upon irradiation at 25 K, an absorption peak ($\text{IS} = 0.02 \pm 0.01 \text{ mm/s}$, $\text{QS} = 0.15 \pm 0.01 \text{ mm/s}$, $\Gamma = 0.44 \pm 0.01 \text{ mm/s}$) of $\text{Fe}^{\text{II}}(\text{ls})$ was significantly reduced and a new doublet peak ($\text{IS} = 0.09 \pm 0.01 \text{ mm/s}$, $\text{QS} = 1.13 \pm 0.01 \text{ mm/s}$, $\Gamma = 0.67 \pm 0.01 \text{ mm/s}$) was observed. This can be assigned to $\text{Fe}^{\text{III}}(\text{ls})$. As a result of the light-induced CT from Fe^{II} to $\text{Co}^{\text{III}}(\text{ls})$, the oxidation state of $\text{Rb}_{0.66}\text{Co}_{1.25}[\text{Fe}(\text{CN})_6]\cdot 4.3\text{H}_2\text{O}$ is changed from $\text{Rb}_{0.66}\text{Co}^{\text{III}}_{0.84}\text{Co}^{\text{II}}_{0.41}[\text{Fe}^{\text{II}}(\text{CN})_6]$ to $\text{Rb}_{0.66}\text{Co}^{\text{II}}_{1.25}[\text{Fe}^{\text{III}}_{0.84}\text{Fe}^{\text{II}}_{0.16}(\text{CN})_6]$. This means that the compound after light illumination has the oxidation states as $\text{Fe}^{\text{III}}(\text{t}_{2g}^5 \text{e}_g^0)\text{—CN—Co}^{\text{II}}(\text{hs}, \text{t}_{2g}^5 \text{e}_g^2)$ ($\nu(\text{CN}) = 2169 \text{ cm}^{-1}$) and $\text{Fe}^{\text{II}}(\text{t}_{2g}^6 \text{e}_g^0)\text{—CN—Co}^{\text{II}}(\text{hs}, \text{t}_{2g}^5 \text{e}_g^2)$ ($\nu(\text{CN}) = 2103 \text{ cm}^{-1}$) which is confirmed by IR data.

Figure 12 shows the UV-vis spectra before and after the light illumination of $\text{Rb}_{0.66}\text{Co}_{1.25}[\text{Fe}(\text{CN})_6]\cdot 4.3\text{H}_2\text{O}$. Upon il-

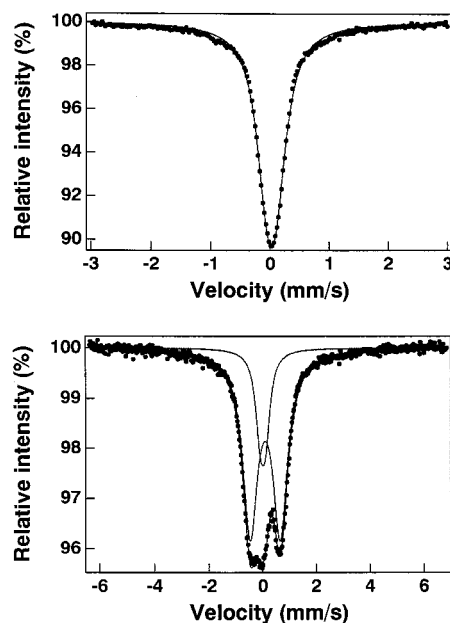


Figure 11. Mössbauer spectra for $\text{Rb}_{0.66}\text{Co}_{1.25}[\text{Fe}(\text{CN})_6]\cdot 4.3\text{H}_2\text{O}$ before (top) and after (bottom) light illumination ($h\nu$) at 25 K.

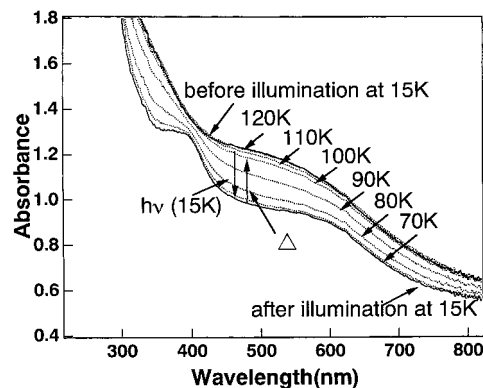


Figure 12. UV-vis spectra for $\text{Rb}_{0.66}\text{Co}_{1.25}[\text{Fe}(\text{CN})_6]\cdot 4.3\text{H}_2\text{O}$ before and after light illumination ($h\nu$) at ca. 15 K (solid line). Temperature dependence of UV-vis spectra after light illumination (dotted line). Temperature is raised from 15 to 120 K. Δ represents thermal treatment.

lumination, the broad CT band was reduced, and the resultant spectra were similar to that of $\text{Co}^{\text{II}}_{1.5}[\text{Fe}^{\text{III}}(\text{CN})_6]\cdot 6\text{H}_2\text{O}$ shown in Figure 4. This change is also explained by the CT process from Fe^{II} to $\text{Co}^{\text{III}}(\text{ls})$. This reveals that the contribution of $\text{Fe}^{\text{II}}(\text{t}_{2g}^6 \text{e}_g^0)\text{—CN—Co}^{\text{III}}(\text{ls}, \text{t}_{2g}^6 \text{e}_g^0)$ is reduced and that of $\text{Fe}^{\text{III}}(\text{t}_{2g}^5 \text{e}_g^0)\text{—CN—Co}^{\text{II}}(\text{hs}, \text{t}_{2g}^5 \text{e}_g^2)$ is increased by light illumination. The increase in the contribution of the paramagnetic components, $\text{Fe}^{\text{III}}(\text{t}_{2g}^5 \text{e}_g^0)\text{—CN—Co}^{\text{II}}(\text{hs}, \text{t}_{2g}^5 \text{e}_g^2)$, enhances the magnetization value and creates the magnetic exchange pathways. Although the theoretical saturation magnetization value for $\text{Rb}_{0.66}\text{Co}^{\text{II}}_{1.25}[\text{Fe}^{\text{III}}_{0.84}\text{Fe}^{\text{II}}_{0.16}(\text{CN})_6]\cdot 4.3\text{H}_2\text{O}$ is $2.9 \mu_B$, the experimental value at 5 T is about $1.32 \mu_B$ at 2 K, indicating some fractions of the paramagnetic component are magnetically isolated due to the presence of the diamagnetic component, $\text{Fe}^{\text{II}}(\text{t}_{2g}^6 \text{e}_g^0)\text{—CN—Co}^{\text{III}}(\text{ls}, \text{t}_{2g}^6 \text{e}_g^0)$.

The temperature dependences of the UV-vis (from 15 to 120 K) and IR (from 15 to 300 K) spectra after the light illumination at 15 K are shown in Figures 12 and 13, respectively. No change was observed below 70 K in the IR and UV-vis spectra, showing that the metastable state, $\text{Fe}^{\text{III}}(\text{t}_{2g}^5 \text{e}_g^0)\text{—CN—Co}^{\text{II}}(\text{hs}, \text{t}_{2g}^5 \text{e}_g^2)$, is maintained below this temperature. Above 80 K, however, the IR peak at 2169 cm^{-1} assigned to $\nu(\text{CN})$ of $\text{Fe}^{\text{III}}(\text{t}_{2g}^5 \text{e}_g^0)\text{—CN—Co}^{\text{II}}(\text{hs}, \text{t}_{2g}^5 \text{e}_g^2)$ was

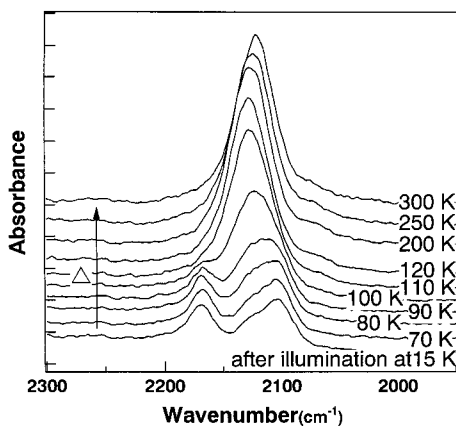


Figure 13. Temperature dependence of CN stretches for $\text{Rb}_{0.66}\text{Co}_{1.25}\text{[Fe(CN)}_6\text{]}\cdot 4.3\text{H}_2\text{O}$ after light illumination ($h\nu$) at ca. 15 K. Temperature is raised from 15 to 300 K. Δ represents thermal treatment.

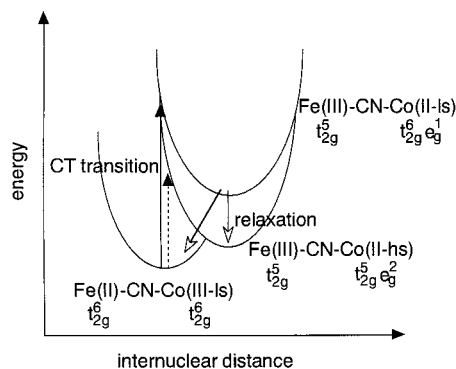
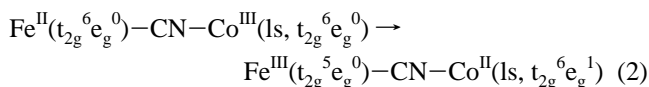


Figure 14. Potential energy diagram of electronic charge-transfer states of $\text{Rb}_{0.66}\text{Co}_{1.25}\text{[Fe(CN)}_6\text{]}\cdot 4.3\text{H}_2\text{O}$.

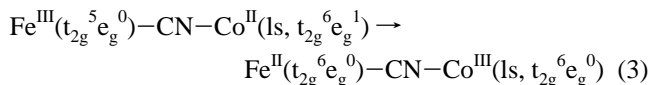
decreased and the peak at 2133 cm^{-1} assigned to $\nu(\text{CN})$ of $\text{Fe}^{\text{II}}(\text{t}_{2\text{g}}^6\text{e}_{\text{g}}^0)\text{--CN--Co}^{\text{III}}(\text{ls}, \text{t}_{2\text{g}}^6\text{e}_{\text{g}}^0)$ was increased. Similarly, the UV–vis spectra showed an increase in the broad CT band above 80 K. Both the IR and UV–vis spectra were completely restored to the original spectra, when the sample was heated to about 120 K, showing that the electron transfer from $\text{Co}^{\text{II}}(\text{hs})$ back to Fe^{III} is thermally induced. The photomagnetization process is schematically illustrated in Figure 14. The potential curve on the left side is the electronic state of $\text{Fe}^{\text{II}}(\text{t}_{2\text{g}}^6\text{e}_{\text{g}}^0)\text{--CN--Co}^{\text{III}}(\text{ls}, \text{t}_{2\text{g}}^6\text{e}_{\text{g}}^0)$. The upper and lower curves on the right side are $\text{Fe}^{\text{III}}(\text{t}_{2\text{g}}^5\text{e}_{\text{g}}^0)\text{--CN--Co}^{\text{II}}(\text{ls}, \text{t}_{2\text{g}}^6\text{e}_{\text{g}}^1)$ and $\text{Fe}^{\text{III}}(\text{t}_{2\text{g}}^5\text{e}_{\text{g}}^0)\text{--CN--Co}^{\text{II}}(\text{hs}, \text{t}_{2\text{g}}^5\text{e}_{\text{g}}^2)$, respectively. Since the energies of the electronic states of $\text{Fe}^{\text{II}}(\text{t}_{2\text{g}}^6\text{e}_{\text{g}}^0)\text{--CN--Co}^{\text{III}}(\text{ls}, \text{t}_{2\text{g}}^6\text{e}_{\text{g}}^0)$ and of $\text{Fe}^{\text{III}}(\text{t}_{2\text{g}}^5\text{e}_{\text{g}}^0)\text{--CN--Co}^{\text{II}}(\text{hs}, \text{t}_{2\text{g}}^5\text{e}_{\text{g}}^2)$ are quite close, the slight change in the ligand field of Co ions can possibly enable the interconversion between the two states.

The light illumination induces the CT from Fe^{II} to $\text{Co}^{\text{III}}(\text{ls})$. To explain this process two possible optical CT transition routes can be considered. One is the direct transition from $\text{Fe}^{\text{II}}(\text{t}_{2\text{g}}^6\text{e}_{\text{g}}^0)\text{--CN--Co}^{\text{III}}(\text{ls}, \text{t}_{2\text{g}}^6\text{e}_{\text{g}}^0)$ to $\text{Fe}^{\text{III}}(\text{t}_{2\text{g}}^5\text{e}_{\text{g}}^0)\text{--CN--Co}^{\text{II}}(\text{hs}, \text{t}_{2\text{g}}^5\text{e}_{\text{g}}^2)$, but this is a spin-forbidden process and may not be seen in the spectrum. Another transition is shown as

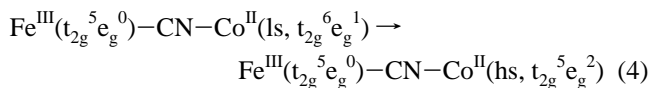


which is spin-allowed and could be observed in the spectrum. The low-spin octahedral $\text{Co}^{\text{II}}(\text{ls})$ complex typically has a strong Jahn–Teller distortion. The absorption coefficient of this CT band is expected not to be large compared with typical CT

transitions, because the corresponding electronic transition is symmetrically forbidden from a $\text{t}_{2\text{g}}$ state of Fe^{II} to an e_{g} state of $\text{Co}^{\text{III}}(\text{ls})$.⁴⁰ After the excitation, some fractions of the excited-state relax to the initial state as

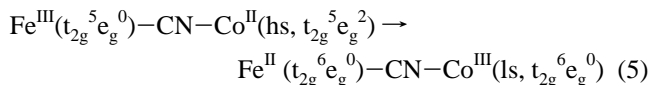


However, an alternative spin-forbidden decay path could be possible due to the spin–orbit coupling as follows:



Because Co^{II} favors a high-spin state, the electronic state of $\text{Fe}^{\text{III}}(\text{t}_{2\text{g}}^5\text{e}_{\text{g}}^0)\text{--CN--Co}^{\text{II}}(\text{hs}, \text{t}_{2\text{g}}^5\text{e}_{\text{g}}^2)$ could be lower than that of $\text{Fe}^{\text{III}}(\text{t}_{2\text{g}}^5\text{e}_{\text{g}}^0)\text{--CN--Co}^{\text{II}}(\text{ls}, \text{t}_{2\text{g}}^6\text{e}_{\text{g}}^1)$ and it forms a metastable state.

The bottoms of the potential wells (x -axis in Figure 14) for $\text{Fe}^{\text{II}}(\text{t}_{2\text{g}}^6\text{e}_{\text{g}}^0)\text{--CN--Co}^{\text{III}}(\text{ls}, \text{t}_{2\text{g}}^6\text{e}_{\text{g}}^0)$ and $\text{Fe}^{\text{III}}(\text{t}_{2\text{g}}^5\text{e}_{\text{g}}^0)\text{--CN--Co}^{\text{II}}(\text{hs}, \text{t}_{2\text{g}}^5\text{e}_{\text{g}}^2)$ are expected to be sufficiently separated, because the interconversion from $\text{Fe}^{\text{II}}(\text{t}_{2\text{g}}^6\text{e}_{\text{g}}^0)\text{--CN--Co}^{\text{III}}(\text{ls}, \text{t}_{2\text{g}}^6\text{e}_{\text{g}}^0)$ to $\text{Fe}^{\text{III}}(\text{t}_{2\text{g}}^5\text{e}_{\text{g}}^0)\text{--CN--Co}^{\text{II}}(\text{hs}, \text{t}_{2\text{g}}^5\text{e}_{\text{g}}^2)$ is accompanied by a large change in the Co–N bond length due to the spin transition of Co ions. The change is estimated to be as large as 0.18 \AA .²⁶ Hence, to induce the back electron transfer as shown



a large reorganization energy is required, which contributes to the potential barrier. Furthermore, this process involves a $\Delta S = 3/2$ transition in Co ions. This reaction is typically spin-forbidden, which also functions as a barrier to the back electron transfer. Therefore, the relaxation involving spin transition results in an increase in the thermal activation energy for the back electron transfer. Consequently, the self-trapping via electron–phonon coupling is the key factor in the extraordinary long-lived metastable state. Note that the light illumination effects for dinuclear compounds with the electronic state of $\text{M}^{\text{II}}\text{--CN--Co}^{\text{III}}$ ($\text{M} = \text{Fe}, \text{Ru}$, etc.) have been investigated,^{32,41} in which the $\text{M}^{\text{III}}\text{--CN--Co}^{\text{II}}$ bonding structure is formed by the photoinduced CT from a $\text{t}_{2\text{g}}$ state of M^{II} to an e_{g} state of Co^{III} . However, these compounds dissociate into two (or more than two) components in solution phase, because Co^{II} is a labile species. In contrast, the $\text{Co}^{\text{II}}(\text{hs})$ state can be maintained in the solid state, allowing the reversible CT between Fe and Co ions.

Finally, we remark on the cooperativity resulting from the intermolecular interactions. As described above, the electron transfer is accompanied by a large change in the Co–N bond length. It is possible that the $\text{Fe}^{\text{III}}(\text{t}_{2\text{g}}^5\text{e}_{\text{g}}^0)\text{--CN--Co}^{\text{II}}(\text{hs}, \text{t}_{2\text{g}}^5\text{e}_{\text{g}}^2)$ moieties are more stabilized when they are surrounded by similar $\text{Fe}^{\text{III}}(\text{t}_{2\text{g}}^5\text{e}_{\text{g}}^0)\text{--CN--Co}^{\text{II}}(\text{hs}, \text{t}_{2\text{g}}^5\text{e}_{\text{g}}^2)$ moieties, because the distortion of the CN networks which arises from the mismatch of the lattice parameters between these two moieties can be avoided. In fact, the strong cooperative interactions in the cobalt–iron cyanide systems can be demonstrated by two phenomena. One is the thermally induced abrupt transition between $\text{Fe}^{\text{III}}(\text{t}_{2\text{g}}^5\text{e}_{\text{g}}^0)\text{--CN--Co}^{\text{II}}(\text{hs}, \text{t}_{2\text{g}}^5\text{e}_{\text{g}}^2)$ and $\text{Fe}^{\text{II}}(\text{t}_{2\text{g}}^6\text{e}_{\text{g}}^0)\text{--CN--Co}^{\text{III}}(\text{ls}, \text{t}_{2\text{g}}^6\text{e}_{\text{g}}^0)$ around room temperature reported for the compounds synthesized via an electrochemical route.⁴² Such abrupt interconversion is observed only when the strong cooperative interactions induce

(40) Braterman, P. S. *J. Chem. Soc. A* **1966**, 1471.

(41) Vogler, A.; Kunkely, H. *Ber. Bunsen-Ges. Phys. Chem.* **1975**, 79, 83.

the growth of the domains of moieties with similar electronic states [$\text{Fe}^{\text{III}}(\text{t}_{2\text{g}}^5\text{e}_{\text{g}}^0)\text{-CN-Co}^{\text{II}}(\text{h}_s, \text{t}_{2\text{g}}^5\text{e}_{\text{g}}^2)$ or $\text{Fe}^{\text{II}}(\text{t}_{2\text{g}}^6\text{e}_{\text{g}}^0)\text{-CN-Co}^{\text{III}}(\text{1s}, \text{t}_{2\text{g}}^6\text{e}_{\text{g}}^0)$] from the nucleation centers. Another is the change in the IR spectra during the interconversion between $\text{Fe}^{\text{III}}(\text{t}_{2\text{g}}^5\text{e}_{\text{g}}^0)\text{-CN-Co}^{\text{II}}(\text{h}_s, \text{t}_{2\text{g}}^5\text{e}_{\text{g}}^2)$ and $\text{Fe}^{\text{II}}(\text{t}_{2\text{g}}^6\text{e}_{\text{g}}^0)\text{-CN-Co}^{\text{III}}(\text{1s}, \text{t}_{2\text{g}}^6\text{e}_{\text{g}}^0)$. If the transition is induced randomly, the $\nu(\text{CN})$ of $\text{Fe}^{\text{III}}(\text{t}_{2\text{g}}^5\text{e}_{\text{g}}^0)\text{-CN-Co}^{\text{III}}(\text{1s}, \text{t}_{2\text{g}}^6\text{e}_{\text{g}}^0)$ as well as the $\nu(\text{CN})$ of $\text{Fe}^{\text{III}}(\text{t}_{2\text{g}}^5\text{e}_{\text{g}}^0)\text{-CN-Co}^{\text{II}}(\text{h}_s, \text{t}_{2\text{g}}^5\text{e}_{\text{g}}^2)$ and $\text{Fe}^{\text{II}}(\text{t}_{2\text{g}}^6\text{e}_{\text{g}}^0)\text{-CN-Co}^{\text{III}}(\text{1s}, \text{t}_{2\text{g}}^6\text{e}_{\text{g}}^0)$ should be observed during the interconversion. However, the $\nu(\text{CN})$ of $\text{Fe}^{\text{III}}(\text{t}_{2\text{g}}^5\text{e}_{\text{g}}^0)\text{-CN-Co}^{\text{III}}(\text{1s}, \text{t}_{2\text{g}}^6\text{e}_{\text{g}}^0)$, which is located

around 2185 cm^{-1} , did not appear in the spectra. This means that the interconversion proceeded via a pronounced domain formation, indicating the existence of the strong cooperative interactions. Thus, it could be thought that the change from $\text{Fe}^{\text{II}}(\text{t}_{2\text{g}}^6\text{e}_{\text{g}}^0)\text{-CN-Co}^{\text{III}}(\text{1s}, \text{t}_{2\text{g}}^6\text{e}_{\text{g}}^0)$ to $\text{Fe}^{\text{III}}(\text{t}_{2\text{g}}^5\text{e}_{\text{g}}^0)\text{-CN-Co}^{\text{II}}(\text{h}_s, \text{t}_{2\text{g}}^5\text{e}_{\text{g}}^2)$ is a phase transition induced by light illumination, which is distinct from that of the conventional photochromic behavior at a single molecule level.

Acknowledgment. We thank T. Nakazawa, T. Takebuta, and K. Tanahashi for their technical support and A. Manivannan for reading the manuscript.

(42) Sato, O.; Einaga, Y.; Iyoda, T.; Fujishima, A.; Hashimoto, K. *J. Phys. Chem. B* **1997**, *101*, 3904.